Evaluation of detailed reaction models for the modeling of double cellular structures in gaseous nitromethane detonation

Dunstan J.Y. Chi* and Karl P. Chatelain† and Deanna A. Lacoste‡
King Abdullah University of Science and Technology (KAUST), Clean Combustion Research Center (CCRC), Thuwal 23955-6900, Saudi Arabia

This study aims at evaluating the performance of three reaction models to reproduce cell size measurements obtained during nitromethane-oxygen and pure nitromethane detonations ($T_1 = 383 - 390$ K, $P_1 = 20 - 100$ kPa, and $\phi = 0.2 - 1.75$). The validation dataset is composed of 47 cell size measurements and includes conditions presenting both single (λ_1 only) and double (λ_1 and λ_2) cellular structures. Zeldovich'-von Neumann-Döring (ZND) simulations are employed to compute the cell size n (λ_n) by utilizing the induction zone lengths ($\Delta_{i,n}$) and a correlation factor (A_n), determined from the Ng method. The main results are: (i) the computed correlation factors appear insensitive to the reaction model and to the type of cells (λ_1 and λ_2), Thus, an averaged correlation factor $A = 37$ could be employed in future studies; (ii) qualitatively, all the models are underestimating λ_1 in most of the conditions but are satisfactory reproducing λ_2 in rich conditions; (iii) quantitatively, Le's model has the lowest error to reproduce the cell sizes (4.3 in average) and the lowest ratio λ_2/λ_1 (near 5 in most conditions).

I. Introduction

The detonation of pure nitromethane (CH_3NO_2) and rich $CH_3NO_2 - O_2$ mixtures present double cellular structures for specific conditions [1, 2]. Experimentally, Presles et al. [1] evidenced their existence using the soot foil technique for several $CH_3NO_2 - O_2$ mixtures and detonation regimes. Later, Sturtzer et al. [2] extended the results of Presles. [1] by providing the evolution of both the main (i.e., the outer ones) and the secondary (i.e., the smaller ones inside the main cell) cells as a function of the experimental conditions. In addition, they also conducted Zeldovich'-von Neumann-Döring (ZND) simulations, using Djebaili-Chaumeix's reaction model [3], to both empirically correlate the cell size (λ) with the induction length (Δ_i) and to identify the role of the two-stage energy release in the double cellular structure formation. Thus, they reported the correlation factors $k_1 = 20$ and $k_2 = 250$ for the secondary ($\lambda = k_1 \times \Delta_i$) and the main ($\lambda = k_2 \times \Delta_i$) cell sizes. More recently, Khasainov et al. [4] confirmed the sensitivity of the double cellular structures to this two-step energy release using a two-step chemical model in one-(1D) and two-dimensional (2D) numerical simulations. Despite the crucial role of nitromethane chemistry in the double cellular structure modeling, no prior validations of nitromethane detailed reaction models for detonation-relevant conditions were carried out in literature. In fact, most of the previous validation works on the nitromethane kinetics [3, 5–11] were performed far from the detonation-relevant conditions of Presles et al. and Sturtzer et al. (i.e., high-temperature and -pressure with no dilution). Thus, an evaluation of the nitromethane reaction models is required prior to enable a more fundamental understanding of the origin of the double cellular structure with high-fidelity numerical simulations.

This works aims at evaluating the performance of three reaction models (Djebaili-Chaumeix et al. [3], Mathieu et al.[6], and Le et al. [12]) to reproduce both the single and the double cellular structures observed during pure CH_3NO_2 and $CH_3NO_2 - O_2$ detonations. The reaction models are evaluated with a validation dataset composed of 47 experimental cell size measurements from both Sturtzer et al. [2] and Presles et al. [1]. All the cell sizes are computed by the Ng method [13] for each condition and model. Error analyses are performed for different sets of conditions and to determine the overall performance of the models.

II. Numerical methods

All the ZND simulations were performed using the *incident shock* reactor model of ANSYS Chemkin-Pro [14]. This reactor model was selected over the classical ZND simulations tools (i.e., ZNDkin [15, 16] or the Shock and detonation

*Visiting Student, Clean Combustion Research Center, KAUST PO box 4700, Thuwal 23955-6900, Saudi Arabia
†Research Scientist, Clean Combustion Research Center, KAUST PO box 4700, Thuwal 23955-6900, Saudi Arabia
‡Associate Professor, Clean Combustion Research Center, KAUST PO box 4700, Thuwal 23955-6900, Saudi Arabia

toolbox (SDT) [17]) due to the large reaction models employed in this study (see the reaction model presentation). The validation of the *incident shock* reactor model is available in [18].

Table 1 presents the three reaction models that we employed in this study: Djebaili-Chaumeix et al. [3], Mathieu et al. [6], and Le et al. [12]. Only a brief presentation is performed in this section and more details can be found in [3, 6, 12]. Djebaili-Chaumeix's reaction model [3] (Chaumeix) is composed of 69 species and 368 reactions. It was validated on shock-tube data relevant to the pyrolysis and oxidation of nitromethane. Among the three models, this reaction model is the only one previously employed in $CH_3NO_2-O_2$ detonation modeling [2]. Mathieu's reaction model [6] is composed of 166 and 1204 reactions, relying on different H_2, NOx, CH_4, and NH_3 submodels available in the literature. It has been validated on a large of set of ignition delays for highly-diluted ($x_{Ar} = 90 - 99\,\%$) $CH_3NO_2-O_2-Ar$ mixtures. Le's reaction model [12] is composed of 1721 and 8011 reactions. This reaction model is the largest and the most recent reaction model among the three. This exhaustive fuel surrogate model compiles a large number of fuel, fuel additives, and pollutants submodels relevant for engine application. Note that dedicated validations of nitroalkane and alkylnitrate submodels were considered during the development of the 2-ethylhexyl nitrate (EHN) reaction model.

Table 1 Selected reaction models

Model name	Number of species	Number of reaction	Reference
Chaumeix	69	368	Djebaili-Chaumeix et al. [3]
Mathieu	166	1204	Mathieu et al. [6]
Le	1721	8011	Le et al. [12]

The validation dataset is presented in Table 2 and is composed of 47 conditions from Presles et al. [1] and Sturtzer et al. [2]. The validation dataset exclusively contains experimental cell size measurements obtained with the soot foil technique for several CH_3NO_2-O_2 and pure CH_3NO_2 mixtures: $T_1 = 383 - 390\,\mathrm{K}$, $P_1 = 20 - 100\,\mathrm{kPa}$, and $\phi = 0.2 - 1.75$. The equivalence ratio (ϕ) was calculated from the relation $\phi = 1.75/(1 + X)$, where X is determined from the initial mixture composition ($CH_3NO_2 + X\,O_2$). Thus, the equivalence ratio of pure nitromethane equals 1.75, which is consistent with the equivalence ratio calculation for monopropellants (i.e., monopropellants are both fuel and oxidizer), when N_2 is considered as a final product. The validation dataset comprises conditions presenting single and double cellular structures for which a single cell size (λ_1) or two cell sizes (λ_1 and λ_2) are reported, respectively. For conditions presenting single cellular structures, the main cell size is referred to as λ_1, while it corresponds to λ_2 for conditions with double cellular structures. For clarity and consistency in this study, the main cell sizes were renamed λ_2 for $\phi \geq 1.3$ in validation 1, 5, and 6.

Table 2 Experimental data employed in the validation dataset

Valid #	Mixture	ϕ	T_1 [K]	P_1 [kPa]	Reference
1	$CH_3NO_2(-O_2)$	0.2 – 1.75	390	50	Presles et al. [1]
2	$CH_3NO_2(-O_2)$	0.2 – 1.75	383	80	Sturtzer et al. [2]
3	$CH_3NO_2-O_2$	0.4	383	30 – 80	Sturtzer et al. [2]
4	$CH_3NO_2-O_2$	1	383	20 – 80	Sturtzer et al. [2]
5	$CH_3NO_2-O_2$	1.4	383	30 – 100	Sturtzer et al. [2]
6	pure CH_3NO_2	1.75	383	30 – 100	Sturtzer et al. [2]

The cell sizes were determined for each condition and reaction model from the Ng's method [13], whose the generalized expression can be defined as follow: $\lambda_n = A_n \times \Delta_{i,n}$, where λ_n refers to the cell size n; A_n corresponds to the semi-empirical correlation factor of the cell size n. A_n is determined from the stability criteria (χ) of the mixture using Equation 1. For clarity, the coefficients presented in Equation 1 are three-digits rounded. The exact coefficients and more details on the determination of χ are available in [13]; $\Delta_{i,n}$ corresponds to the induction length and is determined from its appearance order n in the thermicity profile, see Fig. 1.

$$A_n = 30.466 + \frac{89.554}{\chi} + \frac{-130.793}{\chi^2} + \frac{42.0245}{\chi^3} - 0.029\chi + 1.026 \cdot 10^{-5}\chi^2 - 1.032 \cdot 10^{-9}\chi^3 \quad (1)$$

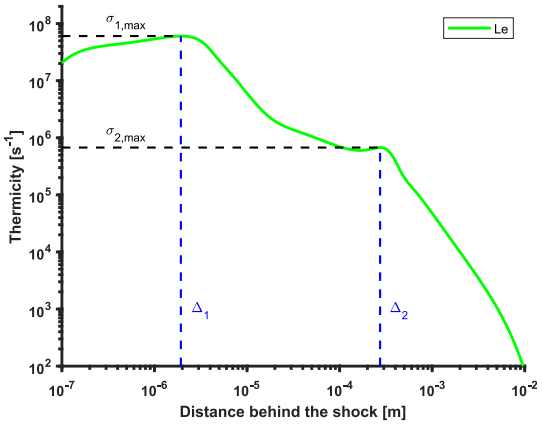

Fig. 1. Thermicity profile as a function of the distance behind the shock, obtained with Le's model with the following mixture: $x_{\mathbf{NM}} = 0.8$, $x_{\mathbf{O_2}} = 0.2$, $T_1 = 383$ K, $P_1 = 100$ kPa, and a Chapman-Jouguet detonation speed. The local maxima (σ_1 and σ_2) are employed to determine the two induction lengths ($\Delta_{1,\mathbf{max}}$ and $\Delta_{2,\mathbf{max}}$), based on their their appearance orders.

Similar to [19, 20], the performance of the models were determined by analyzing the mean errors of the models in different datasets. In this study, we employed the error factor calculation, as employed in [21]. For each experimental condition j, the error factor of the cell size n (EF_n) was determined by $EF_{n,j} = -\lambda_{n,\text{exp.}}/\lambda_{n,\text{sim.}}$, for $\lambda_{n,\text{sim.}} < \lambda_{n,\text{exp.}}$, and by $EF_{n,j} = \lambda_{n,\text{sim.}}/\lambda_{n,\text{exp.}}$, for $\lambda_{n,\text{sim.}} > \lambda_{n,\text{exp.}}$.

Then, the average error on cell size n ($Error_n$) is determined with Equation 2 by averaging the $EF_{n,j}$, obtained for a set of conditions ($j = 1 \rightarrow z_n$) for which $\lambda_{n,\text{sim.}}$ are calculated.

$$Error_n = \frac{1}{z_n} \sum_{j=1}^{z_n} |EF_{n,j}| \tag{2}$$

The global performance of a given model is determined by the mean of the absolute error factors on both λ_1 and λ_2, using Equation 3.

$$\text{Error}_{\text{tot.}} = \frac{1}{z_1 + z_2} \left(\sum_{j=1}^{z_1} |EF_{1,j}| + \sum_{j=1}^{z_2} |EF_{2,j}| \right) \tag{3}$$

III. Results and discussions

A. Ng's parameter results

Table 3 compares the A_n terms obtained for each reaction model against the empirically-determined A_1 and A_2 (i.e., referred to as k_1 and k_2 in [2]) from Chaumeix's model in [2]. Although the newly-determined A_1 are similar (within a factor of 2) to the values from Sturtzer et al. [2], A_2 are near one order of magnitude lower than [2]. This discrepancy seems related to the narrower dataset employed in [2] compared to the Ng method. Table 3 also evidences: (i) the fair consistency of A_n values among the three reaction models; (ii) only Mathieu's model presents more than two thermicity peaks; (iii) the lowest variability is obtained for Le's model; (iv) the A_n values appear constants among the different cell sizes ($A_{n=1\rightarrow4}$). Thus, a single correlation ($A_{\text{avg}} \sim 37$) may be employed in future studies instead of $k_1 = 20$ and $k_2 = 250$, determined by Sturtzer et al. [2]. In the next section, the predicted cell sizes are based on a specific A_n parameters (determined for each model, conditions, and thermicity peak) and are not based on A_{avg}.

Table 3 Summary of the different correlation A_n, with $n = 1 \rightarrow 4$, calculated with the Ng method for each reaction model. Values are compared with the experimentally-determined coefficient from Sturtzer et al. [2]. The variability (±) of each A_n is determined from the standard deviation. *: measured for one condition only.

	A_1	A_2	A_3	A_4	A_{avg}
Exp.-determined [2]	20	250	-	-	-
Chaumeix	37.0 ± 1.0	28.8 ± 7.9	-	-	34 ± 6
Mathieu	34.6 ± 9.1	38.7 ± 6.3	35.1 ± 3.9	43.8*	36 ± 9
Le	38.7 ± 0.7	31.7 ± 4.7	-	-	37 ± 4

B. Validation results

Figs. 2 to 4 present the performance of the three models with our validation dataset (see Table 2). For clarity, linear scales are employed in both Figs. 3a, 3b, 4a, and 4b and the predicted cell sizes smaller than 10 μm are not presented in Figs. 2a and 2b. The following observations are evidenced: (i) None of the models is satisfactory reproducing both λ_1 and λ_2 on the overall dataset. Note that most of the models are satisfactory reproducing the main cell sizes for conditions with double cellular structures (λ_2 for $\phi \geq 1.3$); (ii) Chaumeix's and Le's model satisfactory reproduce the existence of single ((i.e., $\phi < 1.3$) and double ($\phi \geq 1.3$) cellular structures in most of the conditions, except $\phi = 1.0$ for Chaumeix's model and $\phi = 1.3$ for Le's model; (iii) Mathieu's model predicts double cellular structures in conditions for which they were not observed experimentally (e.g., for $\phi \leq 1.2$ in Figs. 2a, 2b, and 3b); Furthermore, this reaction model has more than two thermicity peaks (i.e, up to four) for a large number of conditions (see Fig. 2a and Fig. 4a).

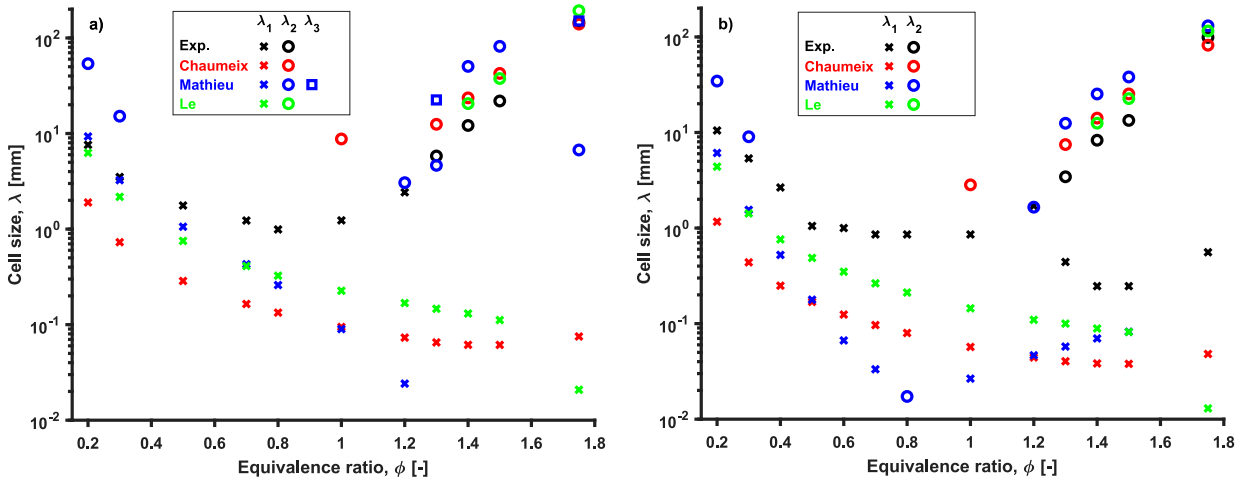

Fig. 2. Experimental (black symbols) and simulated (colored symbols) cell size evolution as a function of the equivalence ratio (ϕ) for the validation cases 1 (in a) and 2 (in b). Chaumeix, Mathieu, and Le's reaction models are in red, blue, and green, respectively.). The conditions in a are from [1]: $\phi = 0.2$ - 1.75), $T_1 = 390$ K, and $P_1 = 50$ kPa. The conditions in b are from [2]: $\phi = 0.2$ - 1.75), $T_1 = 383$ K and $P_1 = 80$ kPa.

Quantitatively, Table 4 summarizes the total error ($Error_{tot}$) calculated for each model, as well as the errors for specific subdatasets. Note that the errors are not calculated for $P \leq 50$ kPa in Fig. 4, as the experimental data are limited by the experimental setup geometry, as stated in [2]. This statement is confirmed by the trends of the modeling results. From Table 4, the following conclusions are drawn: (a) Le's model has the lowest total error (near a factor of 4). This error is significantly lower compared to Chaumeix's and Mathieu's errors (7.4 and 17.3, respectively). Note that most of the error in Le's model is due to λ_1 prediction in Fig. 2b for $\phi = 1.75$; This is due to the high sensibility to determine λ_1 in these conditions (see next section); (b) All the models have a high error at reproducing the secondary cell sizes. The lowest error is near one order of magnitude for Chaumeix model (a factor of 9). The origin of this large errors in λ_1 is mainly to a wide first thermicity peak in most of rich conditions (see next section for more discussions). (c) Mathieu's model has the highest error among the three models and also for every subdataset. This is mainly due to multiple energy

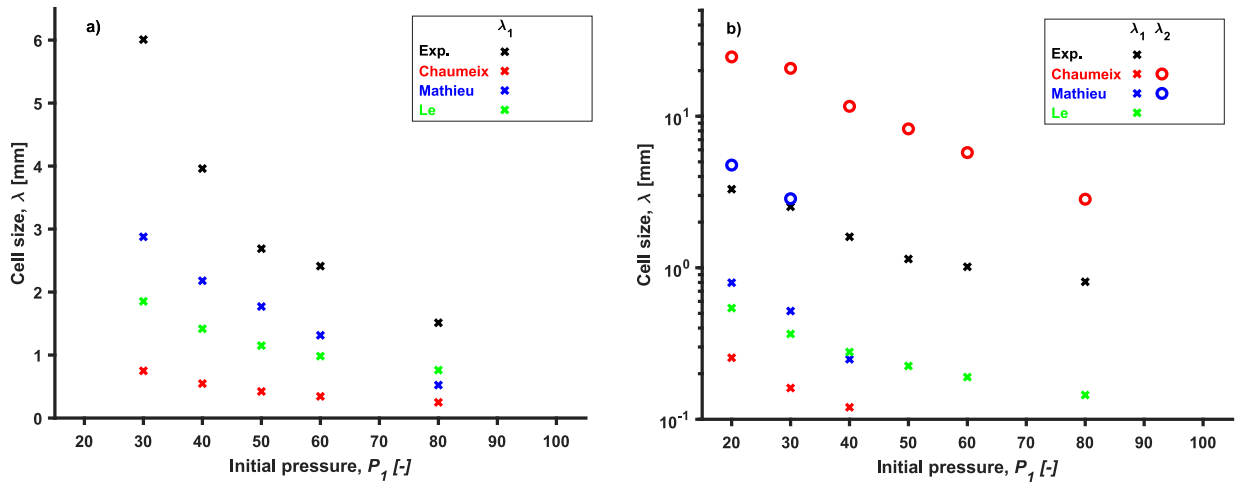

Fig. 3. Experimental (black symbols) and simulated (colored symbols) cell size evolution as a function of the equivalence ratio (ϕ) for the validation cases 3 (in a) and 4 (in b). Chaumeix, Mathieu, and Le's reaction models are in red, blue, and green, respectively.). The conditions in a are from [2]: $\phi = 0.4$, $T_1 = 383$ K and $P_1 = 20$ - 80 kPa. The conditions in b are from [2]: $\phi = 1.0$, $T_1 = 383$ K and $P_1 = 30$ - 80 kPa.

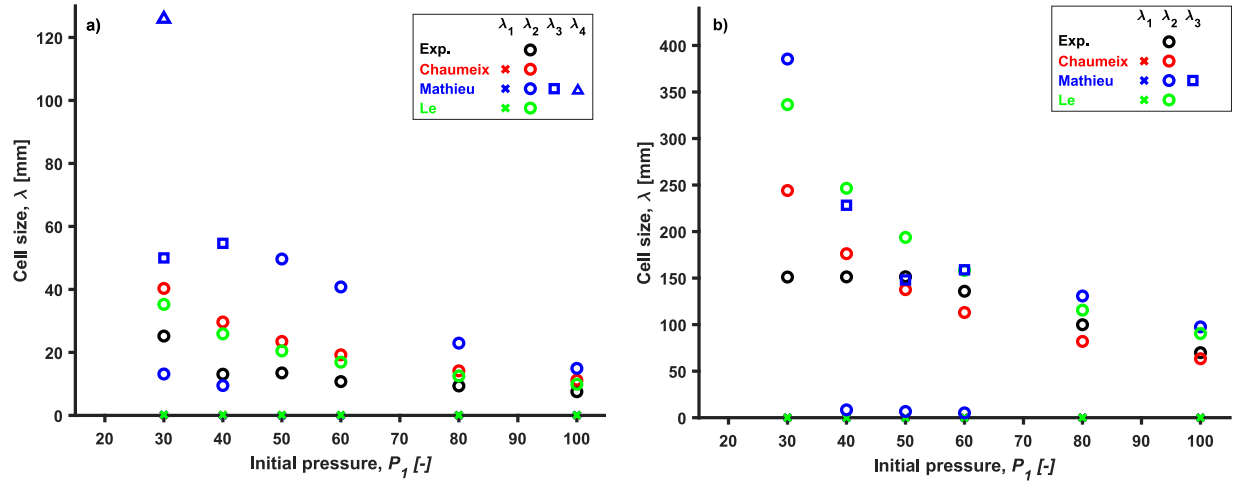

Fig. 4. Experimental (black symbols) and simulated (colored symbols) cell size evolution as a function of the equivalence ratio (ϕ) for the validation cases 5 (in a) and 6 (in b). Chaumeix, Mathieu, and Le's reaction models are in red, blue, and green, respectively.). The conditions in a are from [2]: $\phi = 1.4$, $T_1 = 383$ K and $P_1 = 30$ - 100 kPa. The conditions in b are from [2]: $\phi = 1.75$, $T_1 = 383$ K and $P_1 = 30$ - 100 kPa. On both figures, the modeled λ_1 are below 0.2 μm.

steps, present only in Mathieu's model, for which the first induction lengths are obtained for very short distances (e.g., $\lambda_1 < 10\mu$m in Fig. 2b at $\phi = 0.8$). Further investigations are required to confirm or disregard the relevance of this multi-stage energy release during the detonation of CH_3NO_2(-O_2) mixtures. Note that multi-stage energy releases were also identified for the detonation of DME-O_2-CO_2 mixtures in [18, 22–24].

Note the ratio λ_2/λ_1 can be another interesting validation criteria, as it plays important role in the numerical soot foil results [4]. However, only a brief discussion of this parameter is performed due to the limited number of conditions presenting both λ_1 and λ_2. In average, the three reaction models are overestimating this ratio by more than one order of magnitude. By considering CH_3NO_2-O_2 mixtures only, this average error is reduced to a factor of 16, 16, and 5 for Chaumeix's, Mathieu's, and Le's model, respectively. Thus, Le's model seems the most appropriate reaction model to simulate the double-cellular detonation structures for CH_3NO_2-O_2 mixtures. Nevertheless, large discrepancies between

Table 4 Summary of the error analysis on the three models on specific dataset and on the whole dataset. The underlined number emphasizes the reaction model with the lowest error in each subdataset. *: the main and secondary cell definitions are from Sturtzer et al. [2].

Set of data	$\text{Error}_{\text{tot.,Chaumeix}}$	$\text{Error}_{\text{tot.,Mathieu}}$	$\text{Error}_{\text{tot.,Le}}$
1: Single structure ($\phi \leq 1.2$)	11.6	24.6	<u>4.5</u>
2: Double structure ($\phi \geq 1.3$)	<u>3.0</u>	8.2	4.0
3: Low pressure ($P \leq 50$ kPa)	7.8	9.4	<u>3.6</u>
4: High pressure ($P > 50$ kPa)	7.8	23.7	<u>4.8</u>
5: Main cell*	7.7	17.1	<u>3.4</u>
6: Secondary cell*	<u>8.9</u>	21.5	13.3
All dataset	7.8	17.4	<u>4.3</u>

the numerical soot foils and the experimental ones are expected by employing Le's reaction model, due to the factor of five on λ_2/λ_1.

C. Chemical analyses

Chemical analyses were performed with Le's model in pure CH_3NO_2 condition. Figures 5a and 5b present the thermicity (in black) and the main species contributing to it (colored lines) for the first and second thermicity peak, respectively. In Fig. 5a, the first thermicity peak is very broad (ranging from 0.08 to 8 μm), which results from the contribution of several species at different distances behind the shock, such as CH_3NO_2, NO_2, CH_4, H_2O, CH_2O, NO, CO. In Fig. 5b, the second thermicity peak is sharp and results mainly from the contribution of HCN and CO, as well as the minor contribution of NO and H_2O. Note that similar species contributing to the thermicity profiles were identified among the three reaction models. This indicates that the same most relevant submodels are present in the three reaction models and the lower error of Le's model can only be associated to the kinetics involved in the consumption and production of these species. This analysis is out of the scope of the present study, as it requires detailed reaction pathways and sensitivity analyses with all the models on a large range of conditions.

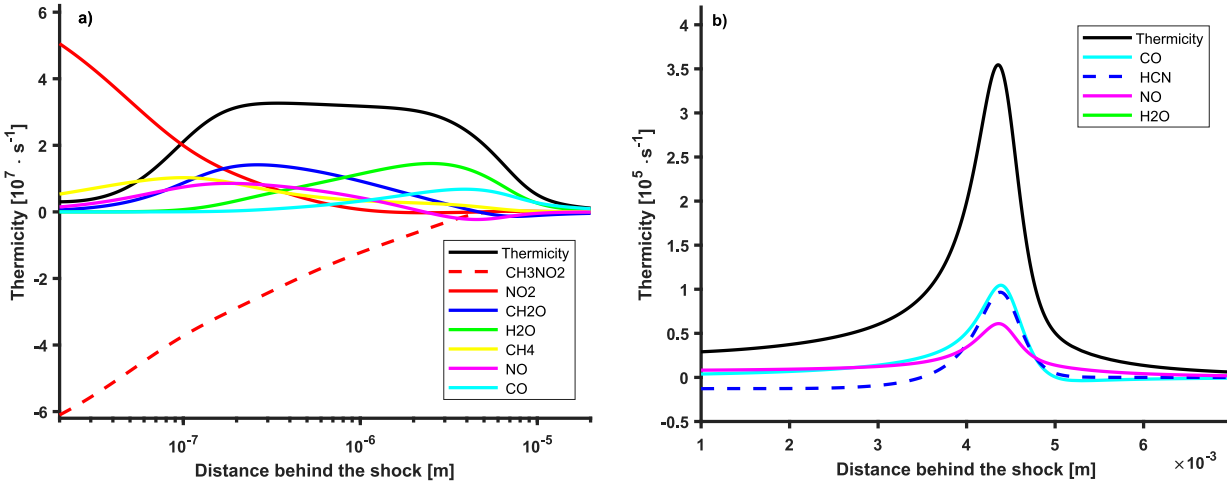

Fig. 5. Species contributing to the first (in a) and second (in b) thermicity peaks as a function of the distance behind the shock. The thermicity profiles and the species contributing to it are represented in black and colored lines, respectively. The resuls were obtained with Le's model for a pure CH_3NO_2 detonation at $T_1 = 383$K and $P_1 = 80$kPa initial conditions.

In addition, Fig. 5 also enabled to identify the origin of the apparent lower performance of both Matthieu's and Le's model at predicting λ_1 for $\phi \geq 1.5$. This lower performance is due to the determination of σ_1 and Δ_1, which are both

very sensitive to the evolution of the species contribution for different conditions. From Fig. 5, Δ_1 will be minimized (ranging from 0.1 to 1 μm) in conditions where CH_2O contribution is strong, while it would be maximized (ranging from 1 to 10 μm) in conditions where H_2O contribution is strong. To mitigate this effect, alternative determination of Δ_i may be required, such as employing the average of the half-maximum distances. Evidencing the applicability of such definition is out of the scope of the present study.

IV. Conclusion

This study evaluated the performance of three reaction models to reproduce single- and double-cellular structure during nitromethane-oxygen and pure nitromethane detonations by using ZND simulations. The performance of Chaumeix's, Mathieu's, and Le's reaction model was evaluated with a validation dataset composed of 47 cell sizes measurements obtained in a large range of conditions: $T_1 = 383 - 390\,\mathrm{K}$, $P_1 = 20 - 100\,\mathrm{kPa}$, $\phi = 0.2 - 1.75$. The Ng method was employed to determine the cell sizes ($\lambda_n = A_n \times \Delta_n$) for each experimental condition and model. The main findings are the following: (i) The correlation factors (A_n), computed from the Ng method, appeared insensitive to the reaction models and to the cell types (i.e., main or secondary). From this result, an average correlation factor ($A_{\mathrm{avg.}} = 37 \pm 4$) can be employed in future studies instead of the values recommended by Sturtzer et al. [2] (ii) Qualitatively, all the models are underestimating λ_1 in most of the conditions. Also, they are satisfactory reproducing the main cell sizes for conditions with double cellular structures (i.e., λ_2 for $\phi \geq 1.3$); (iii) Quantitatively, Le's model has the lowest error to reproduce the cell sizes (4.3 in average) and the lowest ratio λ_2/λ_1 (near 5 in most conditions); (iv) Mathieu's model has the highest error to reproduce the cell sizes in most conditions, due to the presence of thermicity peaks at very short distances; (v) chemical analyses evidenced that the higher performance of Le's model cannot be attributed to a missing submodel in Chaumeix and Matthieu's models. In addition, these analyses also evidenced that the broad first thermicity peak is due to the even contribution of several chemical species. This broad first thermicity peak can partially explain the low performance of most of the models at predicting λ_1. Further analyses are required to identify the origin of the performance of Le's model and the relevance of the multi-stage energy release observed in Mathieu's model. In addition, new experimental data are required to confirm the present validation over a wider range of conditions.

Acknowledgments

The research reported in this publication was supported by funding from King Abdullah University of Science and Technology (KAUST), under award number BAS/1/1396-01-01.

References

[1] Presles, H. N., Desbordes, D., Guirard, M., and Guerraud, C., "Gaseous nitromethane and nitromethane-oxygen mixtures: A new detonation structure," *Shock Waves*, Vol. 6, No. 2, 1996, pp. 111–114. https://doi.org/10.1007/BF02515194.

[2] Sturtzer, M.-O., Lamoureux, N., Matignon, C., Desbordes, D., and Presles, H.-N., "On the origin of the double cellular structure of the detonation in gaseous nitromethane and its mixtures with oxygen," *Shock Waves*, Vol. 14, No. 1, 2005, pp. 45–51. https://doi.org/10.1007/s00193-004-0236-3.

[3] Djebaili-Chaumeix, N., Abid, S., and Paillard, C. E., "Shock tube study of the nitromethane decomposition and oxidation," *21st Symposium on Shock Waves*, Vol. 1, 1997, pp. 121–126.

[4] Khasainov, B., Virot, F., Presles, H.-N., and Desbordes, D., "Parametric study of double cellular detonation structure," *Shock Waves*, Vol. 23, No. 3, 2013, pp. 213–220. https://doi.org/10.1007/s00193-012-0419-2.

[5] Nauclér, J. D., Li, Y., Nilsson, E., Curran, H. J., and Konnov, A. A., "An experimental and modeling study of nitromethane + O 2 + N 2 ignition in a shock tube," *Fuel*, Vol. 186, 2016, pp. 629–638. https://doi.org/10.1016/j.fuel.2016.09.003.

[6] Mathieu, O., Giri, B., Agard, A. R., Adams, T. N., Mertens, J. D., and Petersen, E. L., "Nitromethane ignition behind reflected shock waves: Experimental and numerical study," *Fuel*, Vol. 182, 2016, pp. 597–612. https://doi.org/10.1016/j.fuel.2016.05.060.

[7] Brackmann, C., Nauclér, J. D., El-Busaidy, S., Hosseinnia, A., Bengtsson, P.-E., Konnov, A. A., and Nilsson, E. J., "Experimental studies of nitromethane flames and evaluation of kinetic mechanisms," *Combustion and Flame*, Vol. 190, 2018, pp. 327–336. https://doi.org/10.1016/j.combustflame.2017.12.011.

[8] Weng, J.-J., Tian, Z.-Y., Zhang, K.-W., Ye, L.-L., Liu, Y.-X., Wu, L.-N., Yu, D., Yang, J.-Z., Cao, C.-C., and Zou, J.-B., "Experimental and kinetic investigation of pyrolysis and oxidation of nitromethane," *Combustion and Flame*, Vol. 203, 2019, pp. 247–254. https://doi.org/10.1016/j.combustflame.2019.01.033.

[9] Gao, Z., Yang, M., Tang, C., Yang, F., Yang, K., Deng, F., and Huang, Z., "Measurements of the High Temperature Ignition Delay Times and Kinetic Modeling Study on Oxidation of Nitromethane," *Combustion Science and Technology*, Vol. 192, No. 2, 2020, pp. 313–334. https://doi.org/10.1080/00102202.2019.1565533.

[10] Shrestha, K. P., Vin, N., Herbinet, O., Seidel, L., Battin-Leclerc, F., Zeuch, T., and Mauss, F., "Insights into nitromethane combustion from detailed kinetic modeling – Pyrolysis experiments in jet-stirred and flow reactors," *Fuel*, Vol. 261, 2020, p. 116349. https://doi.org/10.1016/j.fuel.2019.116349.

[11] Mathieu, O., Chaumeix, N., Yamamoto, Y., Abid, S., Paillard, C.-E., Tezuka, T., Nakamura, H., Mulvihill, C. R., and Petersen, E. L., "Nitromethane pyrolysis in shock tubes and a micro flow reactor with a controlled temperature profile," *Proceedings of the Combustion Institute*, Vol. 38, No. 1, 2021, pp. 1007–1015. https://doi.org/10.1016/j.proci.2020.07.132.

[12] Le, M. D., Matrat, M., Amara, A. B., Foucher, F., Moreau, B., Yu, Y., and Glaude, P.-A., "Chemical effects of ferrocene and 2-ethylhexyl nitrate on a low-octane gasoline: An experimental and numerical RCM study," *Proceedings of the Combustion Institute*, Vol. 38, No. 1, 2021, pp. 441–448. https://doi.org/https://doi.org/10.1016/j.proci.2020.06.191.

[13] Ng, H., Ju, Y., and Lee, J., "Assessment of detonation hazards in high-pressure hydrogen storage from chemical sensitivity analysis," *International Journal of Hydrogen Energy*, Vol. 32, No. 1, 2007, pp. 93–99. https://doi.org/10.1016/j.ijhydene.2006.03.012.

[14] ANSYS, "Academic Research Mechanical, Release 20.2," , 2021.

[15] Rojas Chavez, S. B., Chatelain, K. P., Guiberti, T. F., Mével, R., and Lacoste, D. A., "Effect of the excitation line on hydroxyl radical imaging by laser induced fluorescence in hydrogen detonations," *Combustion and Flame*, Vol. 229, 2021, p. 111399. https://doi.org/10.1016/j.combustflame.2021.111399.

[16] Chatelain, K. P., Mével, R., Melguizo-Gavilanes, J., Chinnayya, A., Xu, S., and Lacoste, D. A., "Effect of incident laser sheet orientation on the OH-PLIF imaging of detonations," *Shock Waves*, Vol. 30, No. 7-8, 2020, pp. 689–702. https://doi.org/10.1007/s00193-020-00963-y.

[17] Browne, S., Ziegler, J., and Shepherd, J. E., "Numerical Solution Methods for Shock and Detonation Jump Conditions," , 2008.

[18] Chatelain, K. P., He, Y., Mével, R., and Lacoste, D. A., "Effect of the reactor model on steady detonation modeling," *Shock Waves*, Vol. 31, No. 4, 2021, pp. 323–335. https://doi.org/10.1007/s00193-021-01022-w.

[19] Chatelain, K. P., He, Y., Alharbi, R., Mével, R., Petersen, E. L., and Lacoste, D. A., "Current status of the high-temperature kinetic models of silane: Part I. Pyrolysis," *Combustion and Flame*, Vol. 227, 2021, pp. 526–537. https://doi.org/10.1016/j.combustflame.2020.11.030.

[20] Chatelain, K. P., He, Y., Javoy, S., Mével, R., Petersen, E. L., and Lacoste, D. A., "Current status of the high-temperature kinetic models of silane: Part II. Oxidation," *Combustion and Flame*, Vol. 227, 2021, pp. 538–549. https://doi.org/10.1016/j.combustflame.2020.11.028.

[21] Chatelain, K. P., Mével, R., and Lacoste, D. A., "Correction of Reaction Models Using Collision Limit Violation Analysis," *Combustion and Flame*, Vol. 217, 2020, pp. 346–359. https://doi.org/10.1016/j.combustflame.2020.03.028.

[22] Mével, R., and Gallier, S., "Structure of detonation propagating in lean and rich dimethyl ether–oxygen mixtures," *Shock Waves*, Vol. 28, No. 5, 2018, pp. 955–966. https://doi.org/10.1007/s00193-018-0837-x.

[23] He, Y. Z., and Mével, R., "Effect of hydroxyl radical precursor addition on LTC-affected detonation in DME–O2–CO2mixtures," *Shock Waves*, Vol. 30, No. 7, 2020, pp. 789–798. https://doi.org/10.1007/s00193-020-00974-9.

[24] Han, W., Huang, J., Liang, W., Wang, C., Mével, R., and Law, C. K., "Unsteady propagation of detonation with multi-stage heat release," *Fuel*, Vol. 296, 2021, p. 120666. https://doi.org/10.1016/j.fuel.2021.120666.